Research Article | Vol. 31, No. 26 / 18 Dec 2023 / Optics Express 44680
Optics EXPRESS

Spectrally resolved ultrafast transient dynamics of a femtosecond fiber-feedback optical parametric oscillator

MORITZ FLOESS,* TOBIAS STEINLE, AND HARALD GIESSEN

4th Physics Institute and Research Center SCoPE, University of Stuttgart, Pfaffenwaldring 57, 70569 Stuttgart, Germany
moritz.floess@pi4.uni-stuttgart.de

Abstract: We report on spectrotemporal transient dynamics in a femtosecond fiber-feedback optical parametric oscillator (FFOPO) system. Burst modulation of the pump beam in combination with dispersive Fourier transformation sampling allows to record single-pulse signal spectra at 41 MHz sampling rate. Therefore, each individual pulse of the signal transients can be spectrally resolved. We characterize the signal output behavior for anomalous as well as for normal intra-cavity dispersion. Amongst steady state output we observed period-doubling cycles and other attractors, which occured at higher intra-cavity nonlinearity levels. The experimental findings are supported by numerical simulations, in order to identify the linear and nonlinear effects, which govern the wavelength tuning behavior of this FFOPO system. We find that steady state operation is preferred and that the wavelength tuning stability of the FFOPO dramatically increases when using a normal dispersion feedback fiber.

1. Introduction

Transient dynamics are an inherent part of nonlinear optical systems. Whenever operational conditions change, the system is driven to a new equilibrium state. Stable and repetitive steady state operation may emerge from initially stochastic and chaotic starting conditions. The transient dynamics of numerous different nonlinear systems have been investigated. This includes the buildup of femtosecond mode locking in a Ti:Sapphire oscillator [1], where the transition from cw modes to stable pulsed operation has been demonstrated. These investigations are not restricted to laser oscillators only, parametric light sources have been investigated as well. In particular, the spectrotemporal buildup of a picosecond free-space optical parametric oscillator (OPO) system based on chirped quasi-phase matching has been reported [2]. They observe oscillatory signal output behavior. Furthermore, O'Donnel et al. reported on the spectrotemporal evolution of femtosecond pulses in a fiber-feedback OPO system in the normal and anomalous dispersion regime [3].

Due to stochastic influences the transients are usually non-repetitive events and may fluctuate statistically over time. This imposes challenges to observe these processes, as real-time sampling on the time-scale of a cavity roundtrip is necessary. Therefore, dispersive Fourier transformation is employed, as it provides sufficiently fast sampling and allows to extract spectral information of single-shot events [4,5].

In particular, the starting process of optical parametric oscillation is governed by optical parametric generation (OPG), also known as spontaneous parametric down-conversion, where the conversion of a pump photon into a signal-idler photon pair takes place in the nonlinear crystal [6]. During subsequent cavity roundtrips the spontaneously generated signal is being amplified until the system reaches its equilibrium state, where gain and losses balance each other.

#509472 https://doi.org/10.1364/OE.509472
Journal © 2023 Received 17 Oct 2023; revised 1 Dec 2023; accepted 1 Dec 2023; published 14 Dec 2023

Optics EXPRESS

In this work, we investigate the ultrafast transient dynamics of a femtosecond fiber-feedback OPO (FFOPO) system as well as its equilibrium wavelength tuning characteristics. We demonstrate how normal dispersion feedback strongly suppresses modulation states in the signal output pulse train as well as how it increases the wavelength stability upon changing pump power levels. Throughout this work, the terms "transient" and "equilibrium" are used to denote the signal buildup process and the final state of the output pulse train, respectively. Hereby, the equilibrium may comprise steady state pulse output, i.e., a pulse train of identical pulses, as well as modulated pulse trains such as period-N (PN) cycles. PN cycles are characterized by their signal output being modulated and reproduced after every N^{th} cavity roundtrip. Furthermore, we numerically simulate the FFOPO system in order to identify the dominating effects, which govern the signal output characteristics. In case of anomalous feedback, apart from steady state output, we observe period-doubling and -tripling attractors as well as the formation of limit cycles. In contrast to PN cycles, limit cycles exhibit modulation periods with a non-integer multiple of the roundtrip period [7–9]. Applications, such as nonlinear spectroscopy, sensing, and multi-photon imaging rely on pulse output stability. Therefore, understanding the complex interplay between parametric gain and nonlinear optical feedback with regard to steady state operation and wavelength tuning characteristics is key. Our results provide insights into the transient dynamics of the signal output and its steady state stability.

2. Materials and methods

2.1. Fiber-feedback optical parametric oscillator

The fiber-feedback OPO (FFOPO) is singly-resonant for the signal and is synchronously pumped by an 8-W, 450-fs Yb:KGW bulk oscillator which operates at 1032 nm center wavelength and at a repetition rate of 41 MHz [10], as depicted in Fig. 1(a). The FFOPO is built in linear cavity configuration employing a 10-mm long MgO-doped periodically-poled lithium niobate (PPLN) crystal as parametric gain medium, as illustrated in the detailed inset [11]. A variable output coupler allows to adjust the intra-cavity signal power. In the following, the feedback ratio (FBR) is used as a measure for the intra-cavity signal power. It relates to the output coupling ratio (OCR) via FBR = 1 – OCR.

The largest part of the cavity is wound up in a single-mode fiber, which acts as dispersive and nonlinear feedback element. Hereby, group delay dispersion (GDD) temporally separates the spectral components of the feedback pulse, such that its temporal overlap with the pump pulse effectively determines which wavelength components are being amplified. Hence, wavelength tuning is achieved by adjusting the cavity mismatch between the pump oscillator and the FFOPO cavity, and temperature control of the PPLN crystal for phase matching optimization. The intra-cavity fiber coupling efficiency of the signal amounts to 40%. Given by the linear cavity configuration, two fiber coupling sites are involved per roundtrip, which results in signal power losses of 84% per roundtrip. The FFOPO system can be operated in the anomalous and in the normal dispersion regime employing a SMF-28 or an UHNA7 feedback fiber, respectively. As the feedback fiber provides by far the largest contribution to the overall intra-cavity GDD, swapping the fiber allows to investigate the FFOPO dynamics depending on the intra-cavity dispersion. Note, that the material-specific nonlinear refractive index n_2 is the same for both fibers. Hence, switching between the two fibers allows to isolate and measure the influence of the sign of the intra-cavity GDD. Due to different mode field radii (5 µm for SMF-28, 1.6 µm for UHNA7), ~10 cm of SMF-28 fiber is spliced to both ends of the UHNA7 fiber. This ensures identical mode matching between pump and signal in the gain crystal for both feedback fibers. Nevertheless, the splices cause increased linear transmission losses for the UHNA7 fiber, which amount to 25% at 1550 nm relative to the SMF-28 fiber. Since the feedback fibers are not polarization-maintaining, polarization rotation of the signal feedback may occur depending on the fiber bending. Only p-polarized signal feedback components contribute to the polarization-selective parametric

Optics EXPRESS

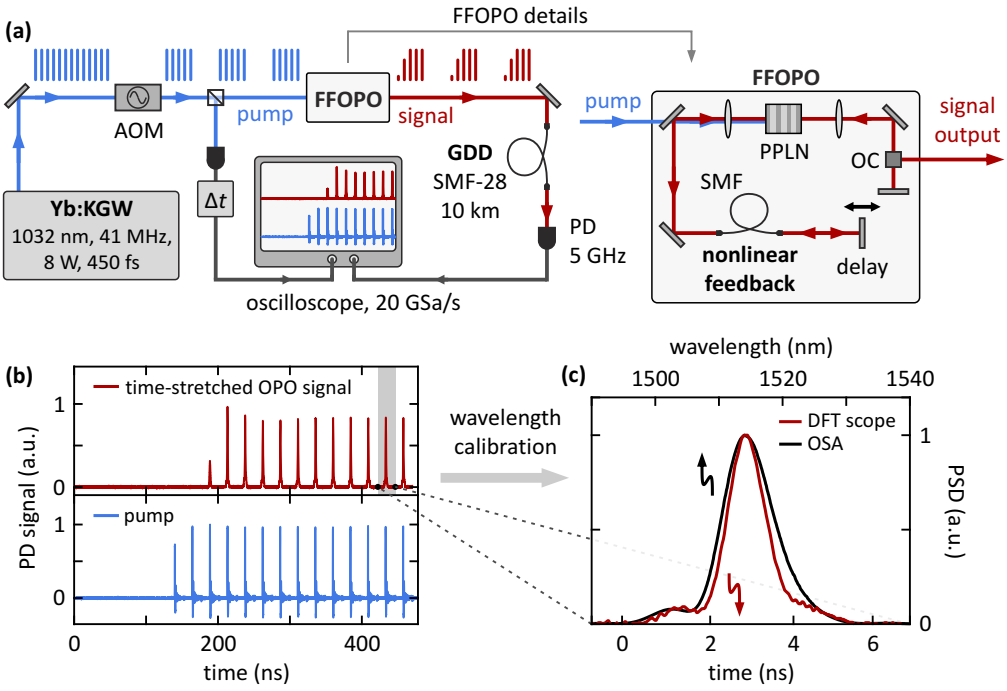

Fig. 1. Pump burst generation and dispersive Fourier transformation (DFT) sampling of the signal transients. (a) An Yb:KGW bulk oscillator (1032 nm center wavelength, 41 MHz repetition rate) provides the pump pulses (blue) for a fiber-feedback optical parametric oscillator (FFOPO). An acousto-optic modulator (AOM) generates pump bursts. The resulting signal transients (red) are recorded using the DFT technique, which employs a 10-km SMF 28 fiber, a 5-GHz photodiode and a 20 GSa/s oscilloscope for sampling of the dispersively time-stretched signal pulses. The corresponding pump burst is recorded as well, where the propagation time difference Δt between pump and signal is compensated in post-processing. Inset: detailed schematic of the synchronously pumped FFOPO based on a MgO:PPLN crystal. A variable output coupler (OC) allows to adjust the intra-cavity signal power level. Wavelength tuning is achieved by changing the crystal temperature and a variable end mirror to adjust the cavity mismatch between the FFOPO and the pump oscillator. Most of the FFOPO cavity consists of a single-mode fiber (SMF), which provides nonlinear optical feedback. (b) Exemplary time traces of the dispersively stretched FFOPO signal and the pump laser after time delay compensation. (c) Absolute wavelength calibration of the single-pulse trace is done by matching it with the average spectrum acquired by an optical spectrum analyzer (OSA).

conversion process (type-0 phase matching), whereas s-polarized components are rejected as cavity losses. In the following experiments, bending and placement of the feedback fibers are therefore carefully optimized in order to minimize polarization rotation.

2.2. *Pump burst generation*

In order to investigate its intrinsic transient behavior, the FFOPO has to be driven from its off-state to full pump power availability within one laser cycle. Therefore, the pump laser needs to be switched on the time scale of the temporal pulse spacing, i.e., 24.4 ns. This is realized using an acousto-optical modulator (AOM) in the pump beam. The focal spot size in the AOM crystal is chosen such that the power throughput is optimized and coating damage is avoided, while maintaining a short rise time of ~20 ns. This is sufficient to generate pump bursts with minimal

Optics EXPRESS

depletion of the first pulse, as depicted in Fig. 1(b). Furthermore, using the first diffraction order of the AOM ensures 100% modulation depth in the pump intensity, such that the FFOPO cavity is emptied completely in between subsequent pump bursts. The driving electronics of the AOM are synchronized to the pump laser repetition rate, in order to ensure precise shuttering between two subsequent pump pulses.

2.3. Single-pulse spectral measurements

In order to quantify the transient dynamics of the FFOPO signal, single-pulse spectra are recorded. This is realized using the dispersive Fourier transformation (DFT) technique. Essentially, a large amount of group delay dispersion (GDD) is exerted on the femtosecond signal pulses, such that the pulses are temporally stretched to the nanosecond regime, where electronic sampling of individual becomes feasible. With this technique, single-pulse spectra can be recorded with an acquisition bandwidth that corresponds to the pulse repetition rate, i.e., 41 MHz in our case.

We realize the DFT scope using a 10-km long single-mode fiber (SMF-28e, Corning). The temporal separation of the spectral components of a 1520 nm signal pulse amounts to 160 ps/nm. This means the initial 350-fs OPO signal pulses with a typical bandwidth of 10–15 nm are temporally stretched to 1.5–3 ns. The transient is sampled in real-time with a fast InGaAs photodiode (5 GHz, Thorlabs, DET08CFC) and a 20-GSa/s oscilloscope (Infiniium DSO9404A). The resulting spectral resolution of $\Delta\lambda = 1$ nm is determined by the overall GDD and the electronic sampling bandwidth. The corresponding pump burst is recorded on a second oscilloscope channel.

As the FFOPO signal pulses propagate through the DFT fiber, their arrival time at the oscilloscope input is delayed by $\Delta t \approx 49$ µs relatively to the corresponding pump burst. Precise temporal matching of the time-stretched signal pulses to the pump burst is done in post processing.

The extraction of the single-pulse spectra from the recorded signal time trace is schematically depicted in Fig. 1(b). The wavelength calibration is carried out in two steps. First, the recorded time axis is mapped onto a relative wavelength axis via the GDD characteristics of the 10-km SMF-28 fiber. In the second step, absolute wavelength calibration is achieved by matching the average of several equilibrium single-pulse traces to a time-averaged spectrum acquired by an optical spectrum analyzer (Ando AQ6317), as depicted in Fig. 1(c).

The quantitative agreement between the single-pulse spectra recorded by the DFT scope and the time-averaged spectra acquired by the optical spectrum analyser decreases for longer wavelengths. This is caused by the formation of donut-shaped transverse modes at longer wavelengths, which cannot be coupled efficiently into the single-mode DFT fiber. As the donut-shaped modes exhibit spectral variations across the beam profile, spectral deviations occur, as demonstrated in Fig. S1 in the Supplement 1. However, the transient duration, relative wavelength shifts, and relative spectral changes in the single-pulse spectra can still be assessed qualitatively.

2.4. Simulations

In order to identify the dominant linear and nonlinear optical effects, which govern the dynamics in the FFOPO cavity, we numerically simulate the signal buildup in the FFOPO system, starting from quantum noise until the output reaches its equilibrium. The simulation uses a 1-dimensional approach, and therefore, spatial effects affecting the beam profile are neglected. Apart from parametric gain, group velocity mismatch between pump, signal, and idler in the PPLN crystal is included. Self-phase modulation (SPM) and dispersion in the feedback fiber, as well as linear cavity losses are considered. The refractive index data for the PPLN crystal used in the simulation are taken from [12,13].

3. Results

In the first step, the output behavior of the FFOPO system in the equilibrium state is characterized, i.e., a continuous pump pulse train drives the FFOPO without burst generation by the AOM. In

Optics EXPRESS

particular, the interplay between the phase matching condition and the cavity mismatch, both of which are control parameters for wavelength tuning, and their impact on the signal output characteristics are investigated. Therefore, the phase matching condition in the PPLN crystal is set to one specific working point, i.e., the crystal temperature and the grating period are kept constant, whereas the cavity mismatch is adjusted to sweep the signal wavelength across the spectral gain window. Figure 2(a) depicts an optical parametric generation (OPG) spectrum (black solid line), which is acquired at an average pump power of 650 mW and at a crystal temperature of 40 °C. The OPG spectrum represents the spectral distribution for which the gain crystal supports parametric amplification of the signal for the given parameter set (crystal length, grating period, crystal temperature) without any optical feedback. Its maximum at 1517 nm marks the spectral position with optimal phase matching. At the short-wavelength slope the simulated OPG spectrum agrees well with the measured spectrum. However, the simulation underestimates the gain towards longer wavelengths, since spatial effects are not considered. In particular, the deviation at longer wavelengths arises from noncollinear phase matching, which will be discussed later.

For these fixed phase matching settings, the signal output power level is measured across the signal wavelength tuning range. As mentioned above, the wavelength is changed only by adjusting the cavity mismatch between the FFOPO and the pump oscillator. Figure 2(a) depicts the signal output power for normal (green) and anomalous dispersion (blue) feedback. For both cases, the output power is measured with an optimized feedback ratio (solid lines), and with a feedback ratio of 25% (dashed lines). The anomalous dispersion feedback results in a maximum output power level of 160 mW, where the normal dispersion feedback yields 125 mW. Maximum output occurs at ~1517 nm, where the measured OPG spectrum exhibits its peak. Owing to its higher linear transmission losses, operation with the UHNA7 feedback fiber results in slightly reduced output power, higher threshold pump power levels, and a narrower wavelength tuning range compared to the SMF-28 fiber.

Figure 2(b) demonstrates the behavior of the signal center wavelength upon pump power variations. The feedback ratio is kept constant at 25%. Each branch corresponds to a fixed cavity mismatch position, for which the pump power is reduced from 650 mW down to the respective threshold power level. As expected, the lowest threshold is reached in the region around the gain maximum. The signal output is strongly asymmetrically extended towards longer wavelengths up to ~1580 nm. In contrast, the simulation yields a symmetrical tuning range, which does not cover signal wavelengths higher than ~1530 nm. The implications of spatial effects on this behavior will be discussed later.

Furthermore, anomalous dispersion feedback tends to cause skewed branches and mode jumps upon pump power variations. In contrast, normal dispersion feedback exhibits stable signal wavelengths for varying pump power levels. Apart from that, a global wavelength shift is observed between the tuning curves of the anomalous and the normal dispersion case. In particular, the tuning curve for anomalous dispersion is shifted to shorter wavelengths with respect to the normal dispersion case. Both findings, wavelength stability and the global wavelength shift, are reproduced by the simulations.

Signal output beam profiles for several different wavelengths across the tuning range are depicted in Fig. 2(c). Fundamental mode profiles are observed only for shorter wavelengths. For increasing wavelengths, donut-shaped beam profiles emerge and gradually become more pronounced. Hereby, in case of normal dispersion feedback the donut mode onset occurs at already shorter wavelengths (~1518 nm) than for anomalous dispersion feedback (~1523 nm).

In the second step, the transient behaviour of the FFOPO signal output is investigated. Therefore, the AOM is used to generate pump bursts, which drive the FFOPO from the off-state into equilibrium. Each individual pulse of the resulting signal transients is spectrally resolved using the dispersive Fourier transformation scope. Figure 3 depicts the spectrotemporal signal

Optics EXPRESS

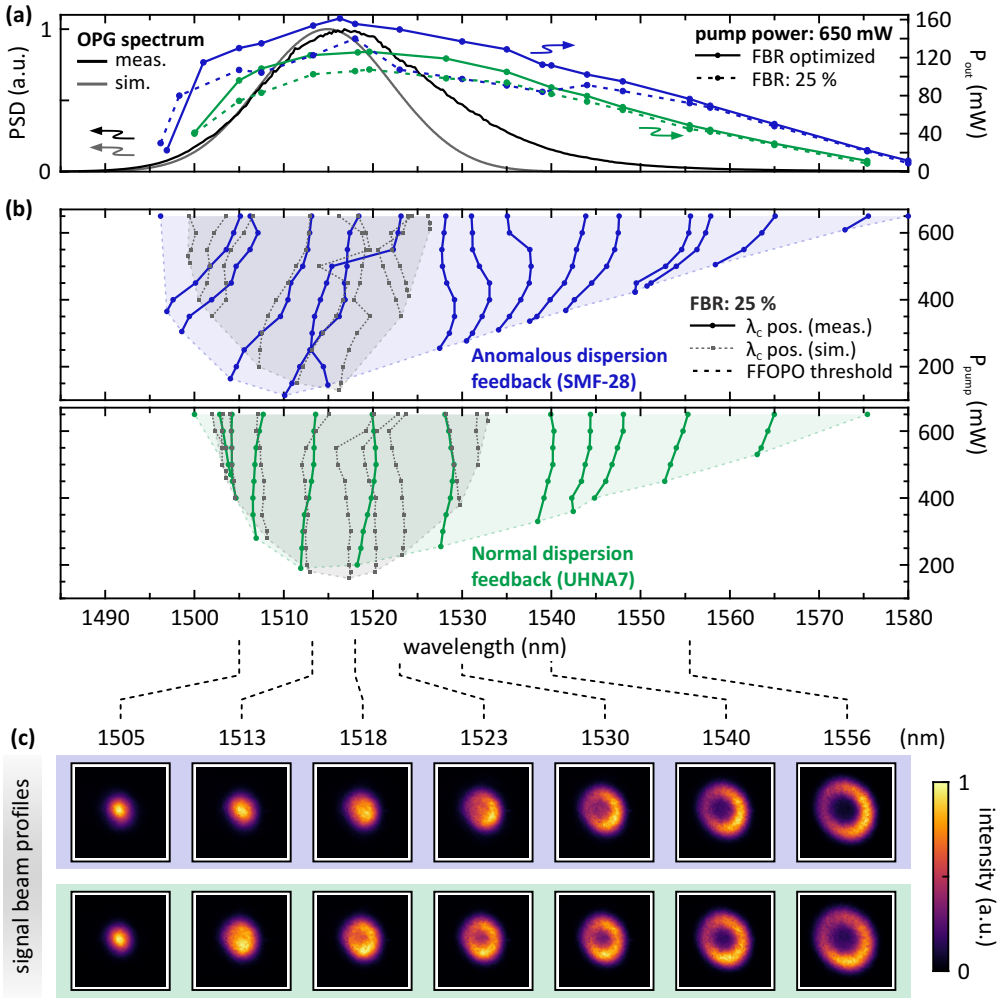

Fig. 2. Wavelength tuning behaviour for normal and anomalous dispersion feedback. (a) Measured OPG spectrum (black) for 650 mW pump power, 40 °C crystal temperature, and fixed poling period, and simulated OPG spectrum (gray). Signal output power for a fixed feedback ratio (FBR) of 25% (dashed lines), and for an optimized FBR (solid lines) for both, anomalous and normal dispersion feedback (blue and green). In both cases, the maximum signal output power level is reached at the gain maximum, i.e., at ~1518 nm. Wavelength tuning is done solely by changing the cavity mismatch. (b) Signal center wavelength depending on the pump power level for anomalous dispersion (upper panel) and for normal dispersion (lower panel) feedback at a FBR of 25%. Simulations are plotted in gray. The threshold pump power level corresponds to the envelope (dashed lines). (c) Signal output beam profiles at different wavelength positions for both, normal and anomalous dispersion feedback. Noncollinear phase matching (NPM) asymmetrically extends the parametric gain towards longer wavelengths, which results in donut-shaped beam profiles. In case of normal dispersion feedback this effect is observed at already shorter wavelengths. The simulations do not include spatial effects, i.e., NPM is neglected. This explains the discrepancy at longer wavelengths between experiment and simulations, as apparent in the OPG spectrum (a) as well as in the wavelength tuning range (b).

Optics EXPRESS

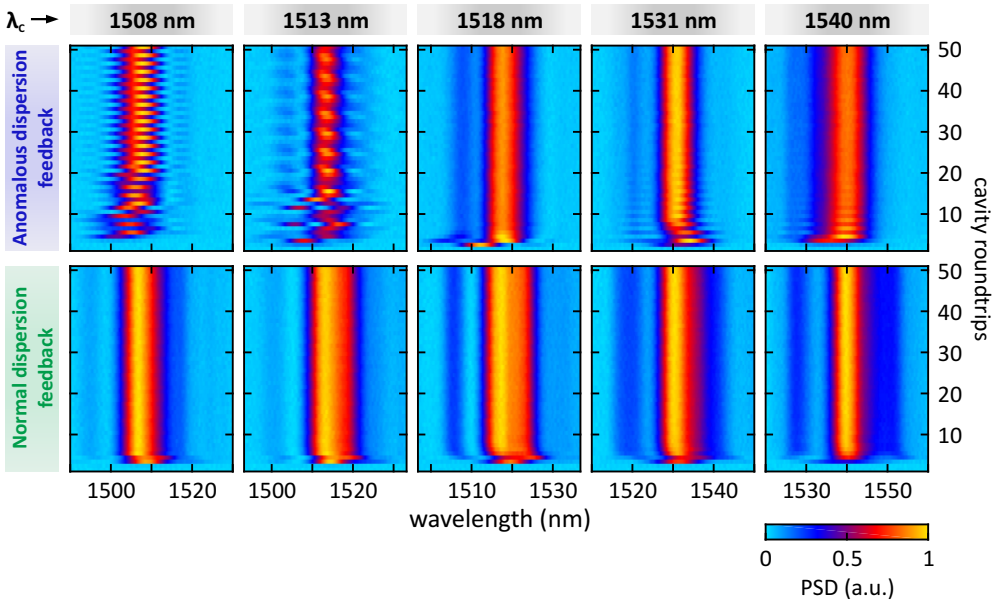

Fig. 3. Spectrotemporal buildup at different wavelengths measured for anomalous and normal dispersion feedback. Wavelength tuning is done by adjusting the cavity mismatch only, while the phase matching condition (poling period and crystal temperature) is kept constant. Constant pump power (650 mW, unmodulated equivalent) and constant feedback ratio (25%). The cavity roundtrip count starts with the first pulse of the corresponding pump burst. Amongst steady states, anomalous dispersion feedback tends to support different equilibrium attractors, such as P2 cycles (1508 nm). Furthermore, transient P2 states (1531 and 1540 nm) or limit cycles (1513 nm) are observed, which eventually subside into steady states. Note, that the transient limit cycle at 1513 nm extends across ~160 roundtrips, which is fully shown in the Supplement 1. In contrast, normal dispersion produces stable steady state output across all wavelengths. A high single-pass gain supports ultrafast transients of <10 roundtrips for normal dispersion, and <20 roundtrips for anomalous dispersion.

buildup process for both, anomalous and normal dispersion feedback, at different wavelengths between 1508 and 1540 nm. The same settings as for Fig. 2(a) are used, i.e., the pump power is set to 650 mW (unmodulated equivalent), the feedback ratio is set to 25%, and wavelength tuning is solely achieved by adjusting the cavity mismatch. Hence, Fig. 3 depicts the transients which correspond to 5 exemplary working points plotted in Fig. 2(a).

The anomalous dispersion feedback tends to support additional attractors rather than steady states only. Hereby, one has to differentiate between the equilibrium attractor, i.e., the state which the signal eventually ends up in, and the transient attractor. In this case, different attractors may occur during the transient process, which finally subside into the equilibrium attractor. At 1508 nm a period-2 (P2) cycle emerges, where a signal pulse is reproduced every 2nd roundtrip. An extremely long transient limit cycle is observed at 1513 nm. Note, that only 50 roundtrips are plotted, which do not cover the entire transient in this case. The corresponding full transient is depicted in Fig. S2 in the Supplement 1. In contrast, normal dispersion seems to stabilize the signal output to steady state operation across all wavelengths.

In both cases, ultrafast transients are observed, despite the high intrinsic intra-cavity losses of >80% per roundtrip. Anomalous dispersion supports transients with typically only <20 roundtrips. In case of normal dispersion feedback, the signal output is equilibrated even faster within <10 roundtrips.

Optics EXPRESS

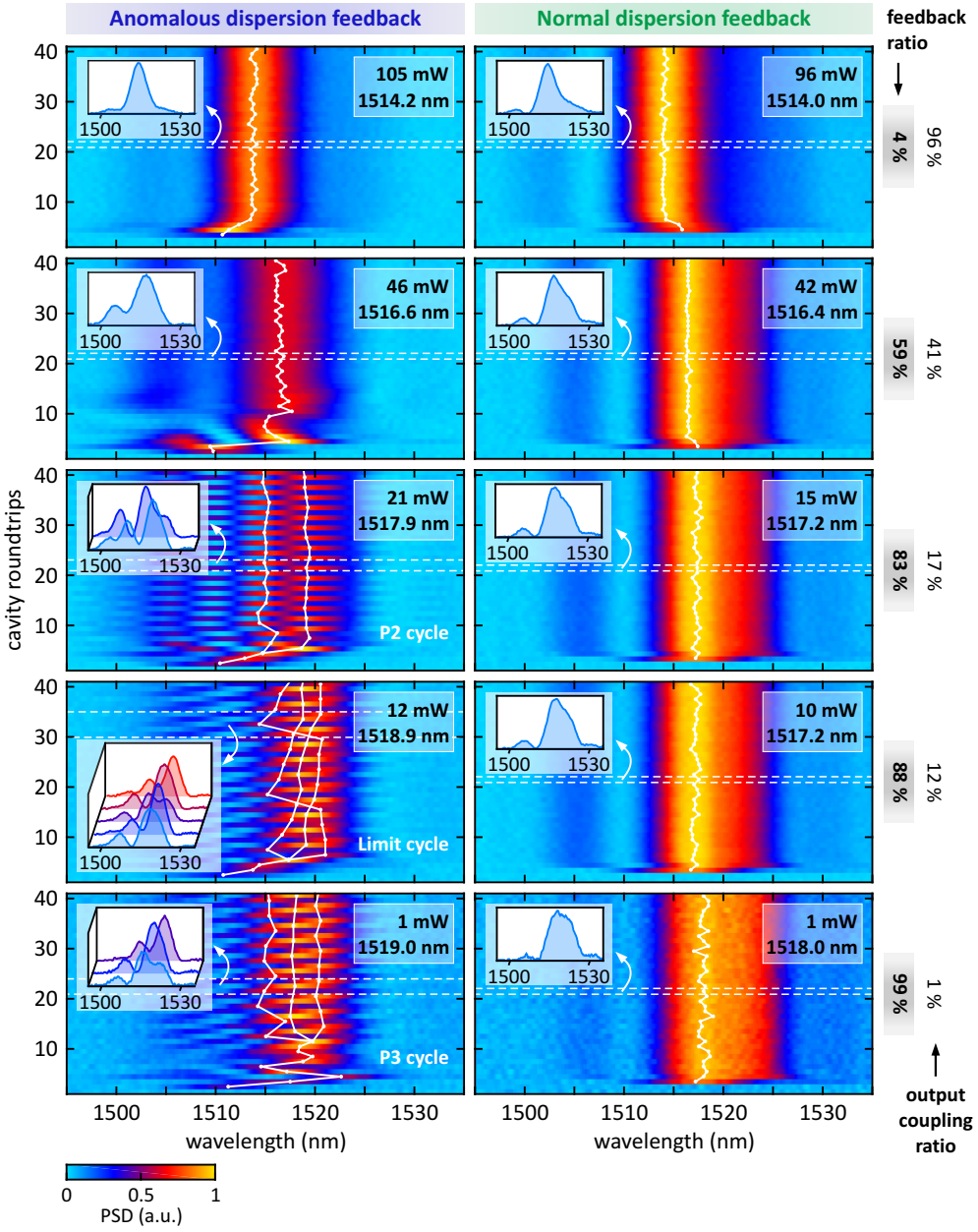

Fig. 4. Influence of the intra-cavity signal power on the spectrotemporal buildup measured for anomalous and normal dispersion feedback. Constant pump power (550 mW, unmodulated equivalent), and constant cavity mismatch. The feedback ratio is increased from 4% to 99%. Therefore, the intra-cavity signal power, and hence, the nonlinearity increases correspondingly. Equilibrium values for the signal output power and the center wavelength are stated for each measurement. Insets: exemplary individual equilibrium spectra as indicated by the horizontal dashed lines. As a guide to the eye, the spectral peak positions of all individual pulses are marked (white dots) and connected (solid white lines) in order to highlight the different emerging attractors.

Optics EXPRESS

In the following, the influence of increasing intra-cavity nonlinearity on the spectrotemporal buildup is investigated. Therefore, the feedback ratio is varied using the variable output coupler. As before, the experiment is carried out for both, anomalous and normal dispersion feedback, as depicted in Fig. 4. The pump power is set to a constant value of 550 mW. The cavity mismatch is fixed, such that the signal output runs at ~1514 nm at minimum feedback ratio.

In accordance with the previous measurement, the equilibrium states are reached within 5–15 cavity roundtrips. For an increasing feedback ratio, the signal output power drops accordingly. In case of anomalous dispersion feedback several different attractors arise for increasing intra-cavity signal power levels. In particular, a P2 cycle is observed for a feedback ratio of 83%, as indicated by the branching spectral peak positions. The inset depicts the two corresponding alternating spectra, which exhibit pronounced spectral modulations. A further increase of the intra-cavity signal power leads to the formation of a limit cycle and eventually a P3 state at feedback ratios of 88%, and 99%, respectively. In contrast, normal dispersion feedback exhibits stable steady state operation even at high intra-cavity nonlinearity, which is favored by the smaller mode field radius of 1.6 µm. In both cases, the center wavelength shifts towards the gain maximum at 1517 nm. Interestingly, for each measured transient the first detected signal pulse is centered around ~1510 nm and ~1517 nm for anomalous and for normal dispersion feedback, respectively. From there, the center wavelength shifts towards its equilibrium value.

4. Discussion

In the following, the most significant effects, which govern the equilibrium and the transient signal output behavior of the FFOPO system shall be discussed. As demonstrated in Fig. 2(a) and (b), the signal wavelength tuning range and the OPG spectrum are asymmetrically extended towards longer wavelengths. This asymmetry is caused by noncollinear phase matching (NPM). Hereby, the phase mismatch at longer wavelengths is compensated by the involved k-vectors adding up in a noncollinear geometry rather than being aligned [14,15]. Thus, NPM provides parametric gain beyond the collinear phase matching bandwidth. This effect is governed by the dispersive properties of the lithium niobate crystal in the infrared spectral region, which restricts the gain extension to the long-wavelength side of the gain window. In k-space the noncollinear geometry forms a donut-shaped profile in the focal spot. Therefore, NPM manifests in the formation of donut-shaped transversal beam profiles in the far field in real space, as depicted in Fig. 2(c). This effect increases towards longer wavelengths, where parametric gain via NPM dominates. The formation of these modes does not gradually build up across several cavity roundtrips. In fact, it results from each single-pass amplification process, since the signal feedback is spatially filtered by the single-mode feedback fiber at each roundtrip. Since the simulation does not consider spatial effects including NPM, the simulated OPG spectrum as well as the tuning range are limited by collinearly phase matched parametric gain, as depicted in Fig. 2(a) and (b), respectively.

Intra-cavity group delay dispersion (GDD) in the feedback fiber introduces a chirp to the feedback pulse, which leads to relative delays in the arrival times in the gain crystal between different spectral components. This has implications on the parametric gain. In particular, leading spectral components experience higher gain than trailing components. This effect is simulated and depicted in Fig. S3 in the Supplement 1. Hence, the sign of the intra-cavity GDD determines whether the short- or the long-wavelength components experience higher gain. Effectively, this GDD-induced temporal gain asymmetry leads to a global wavelength shift of the tuning range between normal and anomalous dispersion operation, as evident from Fig. 2(b). In particular, normal dispersion feedback causes a redshift with respect to anomalous dispersion feedback. This behavior is reproduced by the simulation, which are plotted and shaded in gray. Furthermore, in case of normal dispersion feedback the temporal gain asymmetry favors NPM at already shorter wavelengths than in case of anomalous dispersion feedback. Hence, donut-shaped

Optics EXPRESS

beam profiles already occur at 1518 nm for normal dispersion, whereas for anomalous dispersion they are observed starting from 1523 nm, as depicted in Fig. 2(c).

The signal wavelength stability upon pump power variation strongly differs between operation with anomalous and normal dispersion feedback, as can be assessed from Fig. 2(b). Hereby, the interplay between GDD and SPM in the feedback and parametric gain dictates the output behavior. Additionally to the chirp caused by GDD, SPM induces an up-chirp to the center part of the feedback pulse. Depending on the sign of the GDD, this SPM-induced chirp further enhances (for positive GDD) or partially counteracts (for negative GDD) the GDD-induced chirp. For increasing pump power, the counteracting chirp arising from SPM increases as well. The SPM-induced chirp shifts longer wavelengths towards the temporal gain window of synchronous pumping, i.e., the pump pulse now overlaps with longer-wavelength parts of the signal feedback pulse. Therefore, the center wavelength of the signal output drifts towards higher values for increasing pump power levels. This behavior can be observed in the measurements (skewed blue branches) as well as in the simulation (gray branches). Furthermore, the nonlinear coupling between gain, SPM, and negative GDD leads to wavelength jumps and even crossing branches, where two cavity mismatch positions lead to the same output center wavelength.

In contrast, the SPM-induced chirp acts in the same direction as the chirp induced by positive GDD. On the one hand, this causes the spectral components of the feedback pulse to separate even faster. On the other hand, the accompanying (faster) decrease in peak power in turn terminates the SPM interaction faster as well. The stronger mode confinement (1.6 µm mode field radius) in the UHNA7 fiber, and therefore, the increased SPM response enhances this mechanism even further. This self-terminating mechanism stabilizes the signal output center wavelength against changing SPM contributions, and thus, against varying pump power levels. Both, measurement (green branches) and simulation, exhibit almost no dependence of the signal center wavelength on the pump power level.

The interplay between SPM and GDD also manifests in the transient process on the timescale of individual signal pulses, as shown in Fig. 3. As discussed above, anomalous dispersion feedback gives rise to counteracting chirp contributions from GDD and SPM, which renders the pulse-to-pulse stability sensitive to changing control parameters. In particular, modulation states such as P2 cycles are observed into which the signal output equilibrates. Furthermore, the transients themselves may exhibit clearly patterned attractors, such as P2 states and limit cycles. Interestingly, the observed limit cycle at 1513 nm represents an unstable intermediate state. The initial buildup takes around ~15 roundtrips and launches the limit cycles, which by itself is not long-term stable, but rather subsides into a steady state attractor as the final equilibrium. This happens on a timescale of ~160 roundtrips, which is fully plotted in Fig. S2 in the Supplement 1. In contrast, normal dispersion feedback seems to stabilize the signal output on the pulse-to-pulse timescale as well, i.e., only steady states are observed. As discussed above for the equilibrium output, SPM and positive GDD both exert chirp on the pulse in the same direction, and therefore, stabilize the pulse-to-pulse spectral evolution.

Even though the intra-cavity losses are on the order of 90% per roundtrip including the output coupler [16], the transition from the buildup into equilibrium takes place on the order of 10 roundtrips for normal dispersion feedback, and 20 roundtrips for anomalous dispersion. This ultrafast transient process is facilitated by the extremely high single-pass gain of up to 50 dB [17].

In the next step, the impact of varying intra-cavity signal power on the spectrotemporal buildup will be discussed, as presented in Fig. 4. Hereby, only the output coupling ratio is varied, whereas all other operational parameters are kept constant. As before, the transients exhibit a distinct behavior depending on the sign of the intra-cavity GDD. The gradual increase of the feedback ratio decreases the signal output power from initially ~100 mW at a feedback ration of 4% down to 1 mW at a feedback ratio of 99%. At the same time, SPM in the feedback fiber is being driven more strongly.

Optics EXPRESS

In both cases, the first detected signal pulse is centered around 1510 nm for anomalous dispersion feedback, and around 1517 nm for normal dispersion feedback. This behavior is expected and can be understood as follows: The buildup starts from OPG, which is not influenced by the optical feedback. Therefore, the spectral distribution of the initial seed is the same for all cases, and thus, the starting points are expected to be located always at roughly the same spectral position. Subsequently, the feedback fiber directs the temporally asymmetric gain in one or the other direction, depending on the sign of its GDD. During the subsequent roundtrips the given cavity mismatch enforces a final pump-seed overlap, such that the signal output is directed towards a specific wavelength.

Also, in both cases, the competing effect between optimal parametric gain and the center wavelength dictated by the cavity mismatch can be observed. The center wavelength shifts towards the gain maximum at ~1518 nm for increasing feedback ratios, where gain saturation sets in. At the same time, spectral backconversion starts, i.e., energy conversion from the signal and idler fields back to the pump field via sum-frequency generation [18–20], which manifests in dips in the signal spectrum, as depicted in the inset spectra in Fig. 4. Relatively to these wavelength components, longer signal wavelengths experience higher gain, and therefore, the spectral weight of the output shifts towards the gain maximum at ~1517 nm. This can be clearly seen in the inset spectra in case of normal dispersion output. Hereby, the spectral weight gradually shifts towards longer wavelengths, away from the region of spectral backconversion. Thus, steady state operation is favored even at high intra-cavity nonlinearity levels.

In contrast to that, anomalous dispersion supports higher gain for shorter wavelengths, where spectral backconversion occurs. As evident from the inset spectra, this results in strongly modulated spectra. At some point, this results in different spectra after subsequent amplification cycles, which may lead to the formation of PN states and limit cycles. A P2 state is observed at a feedback ratio of 83%, which is characterized by branching of the spectral peak positions. Accordingly, the P3 cycle at a feedback ratio of 99% exhibits three separate branches of different output spectra. The limit cycle at a feedback ratio of 88%, on the other hand, exhibits crossing branches, which represent the characteristic non-integer period multiplication. Generally, these modulated output attractors are stable over time, given that the ambient conditions are well controlled. Changes in the ambient temperature can suffice to influence the output attractor. In contrast, steady state attractors are usually stable within larger regions of the parameter space given by the operational parameters.

Clearly, the FFOPO signal output exhibits a higher stability when operated with normal dispersion feedback than with anomalous dispersion feedback. This is evident from the wavelength tuning behavior as well as from the dynamics on the pulse-to-pulse timescale. For most applications and measurements, well-defined wavelength tuning characteristics with decoupled control parameters are desirable. Therefore, normal dispersion feedback is the superior choice for this FFOPO system. However, beam profile alterations due to NPM have to be considered and minimized. Therefore, during wavelength tuning the phase matching condition needs to be readjusted carefully, in order to ensure the working point to be located on the short-wavelength side of the spectral gain window.

Nevertheless, the tendency of anomalous dispersion feedback to support P2 cycles may also be employed as a desired feature. In fact, all-optical intensity modulation at the Nyquist frequency is possible without the need for fast electronics, and thus, electronic cross-talk between the modulator and the detection unit is avoided. This scheme can be employed for modulation spectroscopy applications, such as stimulated Raman scattering spectroscopy as demonstrated in [21].

Optics EXPRESS

5. Conclusion

We have presented the transient signal dynamics in a femtosecond FFOPO system. Using pump bursts allows to drive the FFOPO from the cold-cavity state into equilibrium. The resulting ultrafast signal transients have been recorded with the dispersive Fourier transform technique, which provides spectral resolution for each individual signal pulse. We have demonstrated the impact of intra-cavity normal and anomalous dispersion in the optical feedback on the pulse-to-pulse dynamics, and on the wavelength tuning behavior. Anomalous dispersion feedback gives rise to oscillatory output pulse patterns, such as period-N states and limit cycles. By supporting the experimental data with numerical simulations, we have identified SPM and GDD to be the dominating effects which govern the dynamics of FFOPO system. Noncollinear phase matching asymmetrically extends the wavelength tuning range at the expense of donut-shaped signal beam profiles.

We conclude that normal dispersion feedback stabilizes the pulse-to-pulse output, such that steady state operation is preferred. Additionally, wavelength tuning exhibits uncoupled control parameters and is free of mode jumps and wavelength drifts upon varying pump power levels. This renders operation in the normal dispersion regime to be preferable for most applications.

Funding. European Research Council (PoC 3DPRINTEDOPTICS); Carl-Zeiss-Stiftung; Deutsche Forschungsgemeinschaft (GRK 2642); Integrated Quantum Science and Technology (IQST); Terra Incognita University of Stuttgart; Baden-Württemberg Stiftung; Bundesministerium für Bildung und Forschung.

Acknowledgments. We thank Abdullah Alabbadi for his help with the fiber preparation and for valuable discussions.

Disclosures. The authors declare no conflicts of interest.

Data availability. Data underlying the results presented in this paper are not publicly available at this time but may be obtained from the authors upon reasonable request.

Supplemental document. See Supplement 1 for supporting content.

References

1. G. Herink, B. Jalali, C. Ropers, *et al.*, "Resolving the build-up of femtosecond mode-locking with single-shot spectroscopy at 90 MHz frame rate," Nat. Photonics **10**(5), 321–326 (2016).
2. D. Descloux, C. Laporte, J. Dherbecourt, *et al.*, "Spectrotemporal dynamics of a picosecond OPO based on chirped quasi-phase-matching," Opt. Lett. **40**(2), 280–283 (2015).
3. C. O'Donnell, S. Kumar, T. Paoletta, *et al.*, "Widely tunable femtosecond soliton generation in a fiber-feedback optical parametric oscillator," Optica **7**(5), 426–433 (2020).
4. P. Kelkar, F. Coppinger, A. Bhushan, *et al.*, "Time domain optical sensing," Electron. Lett. **35**(19), 1661–1662 (1999).
5. K. Goda and B. Jalali, "Dispersive Fourier transformation for fast continuous single-shot measurements," Nat. Photonics **7**(2), 102–112 (2013).
6. G. Arisholm, "Quantum noise initiation and macroscopic fluctuations in optical parametric oscillators," J. Opt. Soc. Am. B **16**(1), 117–127 (1999).
7. M. Kues, N. Brauckmann, T. Walbaum, *et al.*, "Nonlinear dynamics of femtosecond supercontinuum generation with feedback," Opt. Express **17**(18), 15827–15841 (2009).
8. N. Brauckmann, M. Kues, T. Walbaum, *et al.*, "Experimental investigations on nonlinear dynamics in supercontinuum generation with feedback," Opt. Express **18**(7), 7190–7202 (2010).
9. M. Kues, N. Brauckmann, P. Groß, *et al.*, "Basic prerequisites for limit-cycle oscillations within a synchronously pumped passive optical nonlinear fiber-ring resonator," Phys. Rev. A **84**(3), 033833 (2011).
10. A. Steinmann, B. Metzger, R. Hegenbarth, *et al.*, "Compact 7.4 W femtosecond oscillator for white-light generation and nonlinear microscopy," *CLEO: 2011 - Laser Science to Photonic Applications*, Baltimore, MD, 2011, pp. 1–2.
11. T. Steinle, F. Mörz, A. Steinmann, *et al.*, "Ultra-stable high average power femtosecond laser system tunable from 1.33 to 20 µm," Opt. Lett. **41**(21), 4863–4866 (2016).
12. R. DeSalvo, A. A. Said, D. J. Hagan, *et al.*, "Infrared to Ultraviolet Measurements of Two-Photon Absorption and n_2 in Wide Bandgap Solids," IEEE J. Quantum Electron. **32**(8), 1324–1333 (1996).
13. D. H. Jundt, "Temperature-dependent Sellmeier equation for the index of refraction, n_e, in congruent lithium niobate," Opt. Lett. **22**(20), 1553–1555 (1997).
14. P. Tzankov, J. Zheng, M. Mero, *et al.*, "300 µJ noncollinear optical parametric amplifier in the visible at 1 kHz repetition rate," Opt. Lett. **31**(24), 3629–3631 (2006).
15. G. Cirmi, D. Brida, C. Manzoni, *et al.*, "Few-optical-cycle pulses in the near-infrared from a noncollinear optical parametric amplifier," Opt. Lett. **32**(16), 2396–2398 (2007).

Optics EXPRESS

16. M. Floess, T. Steinle, I. Gerhardt, *et al.*, "Femtosecond tunable light source with variable repetition rate between 640 kHz and 41 MHz with a 130 dB temporal pulse contrast ratio," Opt. Express **30**(1), 1–11 (2022).
17. M. Floess, T. Steinle, and H. Giessen, "Burst-mode femtosecond fiber-feedback optical parametric oscillator," Opt. Lett. **47**(3), 525–528 (2022).
18. G. Arisholm, G. Rustad, and K. Stenersen, "Importance of pump-beam group velocity for backconversion in optical parametric oscillators," J. Opt. Soc. Am. B **18**(12), 1882–1890 (2001).
19. C. Phillips and M. Fejer, "Efficiency and phase of optical parametric amplification in chirped quasi-phase-matched gratings," Opt. Lett. **35**(18), 3093–3095 (2010).
20. J. Moses, N. Flemens, and X. Ding, "Back-conversion suppressed parametric frequency conversion for ultrawide bandwidth and ultrahigh efficiency devices," Proc. SPIE 11264, Nonlinear Frequency Generation and Conversion: Materials and Devices XIX, 112640B (2020).
21. T. Steinle, M. Floess, A. Steinmann, *et al.*, "Stimulated Raman Scattering Microscopy with an All-Optical Modulator," Phys. Rev. Appl. **11**(4), 044081 (2019).